ORIGINAL PAPER

Sulfidation of Supported Ni, Mo and NiMo Catalysts Studied by In Situ XAFS

Dorotea Gajdek[1,2] · Lucy Idowu Ajakaiye Jensen[3] · Valérie Briois[4] · Christian Hulteberg[3] · Lindsay R. Merte[1,2] · Sara Blomberg[2,3]

Abstract

Active sites in Mo-based hydrotreating catalysts are produced by sulfidation. To achieve insights that may enable optimization of the catalysts, this process should be studied in situ. Herein we present a comparative XAFS study where the in situ sulfidation of Mo/δ-Al$_2$O$_3$ and Ni/δ-Al$_2$O$_3$ is compared to that of δ-Al$_2$O$_3$ supported NiMo catalysts with different NiMo ratios. The study also covers the comparison of sulfidation of Ni and Mo using different oxide supports as well as the sulfidation conditions applied in the reactor. The XAFS spectra confirms the oxide phase for all catalysts at the beginning of the sulfidation reaction and their conversion to a sulfidized phase is followed with in situ measurements. Furthermore, it is found that the monometallic catalysts are less readily sulfidized than bimetallic ones, indicating the importance of Ni-Mo interactions for catalyst activation. Mo K-edge XAFS spectra did not show any difference related to the support of the catalyst or the pressure applied during the reaction. Ni K-edge XAFS spectra, however, show a more complete sulfidation of the Ni species in the catalyst when SiO$_2$ is used as a support as compared to the Al$_2$O$_3$. Nevertheless, it is believed that stronger interactions with Al$_2$O$_3$ support prevent sintering of the catalyst which leads to its stabilization. The results contribute to a better understanding of how different parameters affect the formation of the active phase of the NiMo catalysts used in the production of biofuel.

Keywords Bimetallic catalysts · XAFS · Industrial catalysts · X-ray techniques · NiMo catalyst · Sulfidation

1 Introduction

The transition from fossil-based fuels to the more sustainable production of biofuel is an important step to reach a net-zero carbon footprint. The amount of greenhouse gas (GHG) emissions is still increasing worldwide, and the transport sector stands for a large part of these emissions. In particular, the aviation and maritime sectors are expected to increase GHG emissions in the upcoming years [1].

The replacement of fossil fuels with biofuels is especially important for aviation, where this sector may be the most difficult sector to electrify. Traditionally, the production of fossil-based fuel relies on hydrotreatment processes where the reduction of sulfur and nitrogen in hydrodesulfurization (HDS) and hydrodenitrogenation (HDN) respectively are important catalytic reactions. The alternative feedstocks, however, differ in chemical composition from fossil-based feedstocks, in particular having high oxygen content which has to be reduced to produce high-quality fuel. Transition metals such as Pd and Pt have been suggested as potential catalysts in the catalytic hydrotreatment of biomass, but transition metals are expensive and highly susceptible to sulfur poisoning [3]. For the hydrotreatment processes, Molybdenum (Mo) is a well-established and efficient catalyst and is widely used in the petrochemical industry [2]. Mo-based catalysts are also efficient in the hydrodeoxygenation (HDO) process for biomass [4–7] and so, are promising for this application as well.

✉ Sara Blomberg
 sara.blomberg@chemeng.lth.se

1 Department of Materials Science and Applied Mathematics, Malmö University, 205 06 Malmö, Sweden

2 NanoLund, Lund University, Box 118, 211 00 Lund, Sweden

3 Department of Chemical Engineering, Lund University, Box 118, 221 00 Lund, Sweden

4 Synchrotron SOLEIL, UR1-CNRS, L'Orme des Merisiers, Saint-Aubin, BP 48, 91192 Gif-sur-Yvette Cedex, France

Springer

Traditionally, the precursor of the Mo-based catalyst is MoO_3 but during exposure to a sulfur-containing feedstock, such as crude oil, the Mo oxide transforms into a more active Mo sulfide. Today, however, some refineries are co-feeding fossil-based feedstock with bio-based feedstock to produce renewable fuel. The co-feeding with more oxygen-containing feedstock, such as biomass, changes the sulfidation conditions in the reactor and may result in a less active catalyst. Hence, it is desirable to achieve detailed knowledge about the optimized condition for the activation process to be able to control and stabilize the most active phase. The active phase is believed to consist of single-layer MoS_2 nanoclusters, whose edges provide active sites for hydrotreating reactions [8–11]. Furthermore, the transformation into the active MoS_2 has shown to be dependent on the oxide structure and oxidation state of the Mo precursor, and the sulfidation of MoO_3 is reported to be more facile as compared to the sulfidation of Mo species with lower oxidation states such as MoO_2 [12]. The active site of the MoS_2 islands is linked to sulfur vacancies, which creates reactive coordinated unsaturated sites (CUS) at the edges of the islands. The number of active sites per gram Mo can, due to that, be increased by decreasing the size of the islands, resulting in a more active catalyst [13, 14].

The size of the MoS_2 islands is highly dependent on the interaction with the support, which is, therefore, an important parameter when producing the Mo-based catalyst. Al_2O_3 is the most common support and due to the high surface area, the γ-phase is widely used. An advantage of using alumina over many other supporting oxides is that the active metal is well dispersed over the large area of the alumina support and sintering of the active material is inhibited by the strong interaction with the support [15]. The alumina is also active in the hydrocracking of heavy oils, which is an advantage in some hydrotreatment processes, but it may also contribute to coke formation. In this study, however, the δ-phase of the Al_2O_3 is used, motivated by the large pores (compared to the γ-phase), which is an advantage when large molecular complexes, such as biomass compounds, should be upgraded in the catalytic process [16–18]. For a better understanding of the effect of the support in the sulfidation process, SiO_2 support is used for comparison, in this study. To further improve the catalytic performance, metal promoters can be added, where Ni and Co are the most commonly used, but for the HDO process, Ni has been suggested to be the most efficient promoter [19–23]. The promoters donate electrons to Mo, which weakens the bond to the sulfur resulting in more facile CUS formation [20]. The promoting effect of Ni in Mo catalysts has also been demonstrated in reduction experiments where Ni lowers the temperature of the Mo^{6+} to Mo^{4+} reduction step [24, 25]. This is clear evidence that the interaction between Ni and Mo changes the properties of the catalysts, and it has previously been shown that the Ni:Mo ratio affects the activity of the catalyst [20, 26, 27].

X-ray absorption fine structure spectroscopy (XAFS) is a powerful technique for studying in situ materials characterization over a wide range of conditions [28, 29]. The technique is performed using hard X-rays and is traditionally divided into two regions. The region near the absorption edges (XANES) gives information about oxidation states and coordination chemistry of the species which can be used as a chemical fingerprint to identify specific phases. The second region is extended X-ray absorption fine structure spectroscopy (EXAFS), which makes use of the fine structure far above the absorption edge and provides information about the structure of the observed species due to the contributions of local photoelectron scattering [30–32].

In the present study, we investigate the sulfidation process of Mo-based catalysts in situ, using Quick- XAFS at the ROCK beamline at the Soleil synchrotron, which allows for rapid alternation between two edges. Due to the high temporal resolution using the edge-jumping method, it is possible to follow the transition from the oxide precursor to the active sulfide phase while characterizing both the Mo and the promoter metal. We have acquired XAFS spectra at the Mo K- and Ni K-edges in situ during sulfidation for a series of catalysts including pure Mo and Ni, mixed catalysts with differing Ni:Mo ratios, and NiMo catalysts on both Al_2O_3 and SiO_2 supports. We furthermore investigated the influence of the total gas pressure during sulfidation, as this is frequently a constraint for in situ measurements.

2 Experimental Methods

2.1 Sample Preparation

Catalyst materials used for this study were prepared using incipient wetness impregnation of δ-alumina (Al_2O_3) and silica (SiO_2) supports following procedures from Blomberg et al. [33]. Surface area of supports has been determined from nitrogen physisorption using the Brunauer–Emmett–Teller (BET) method. BET surface areas of the δ-Al_2O_3 and SiO_2 support materials were determined to be 121 m^2/g and 250 m^2/g respectively. The notations of the prepared samples, supports used and weight percent (wt%) of Ni and Mo for each sample are shown in Table 1. Catalysts S1–S3 were prepared by impregnation with an aqueous solution of ammonium heptamolybdate tetrahydrate ($H_{24}Mo_7N_6O_{24} \times 4H_2O$) which resulted in nominal loading of 8 wt% of elemental Mo on the support. Following impregnation, the catalysts were aged at room temperature for 4 h, then dried for 15 h at 120 °C, and finally calcined for 4 h at 500 °C. Ni was impregnated onto Mo-containing catalysts using an acidic aqueous solution containing citric acid monohydrate and

Table 1 Prepared catalysts with details of the used support, measured metal loading in wt% from EDX, nominal metal loadings, measured Ni/Mo ratios (at.%) and total pressure used for measurements

Sample	Catalyst type	Support	Wt% Ni measured (nominal)	Wt% Mo measured (nominal)	Measured Ni/Mo molar ratio	Pressure (bar)
S1	NiMo/δ-Al$_2$O$_3$	δ-Al$_2$O$_3$	2.4 (3.4)	7.0 (8.0)	0.55	10
S2	NiMo/δ-Al$_2$O$_3$	δ-Al$_2$O$_3$	2.4 (3.4)	7.0 (8.0)	0.55	2
S3	NiMo/SiO$_2$	SiO$_2$	1.2 (3.4)	9.0 (8.0)	0.22	10
S4	NiMo/δ-Al$_2$O$_3$	δ-Al$_2$O$_3$	2.7 (6.0)	5.0 (4.9)	0.88	10
S5	Ni/δ-Al$_2$O$_3$	δ-Al$_2$O$_3$	8.9 (8.4)	0 (0.0)	–	10
S6	Mo/δ-Al$_2$O$_3$	δ-Al$_2$O$_3$	0 (0.0)	13 (14)	–	10

nickel nitrate hexahydrate (N$_2$NiO$_6$ x H$_2$O) with nominal loading of 3.4 wt% elemental Ni on the support.

Catalyst S4 was prepared on δ-Al$_2$O$_3$ support using the same procedure as the first three catalysts with the difference in wt% of Mo and Ni. Catalyst S5 was prepared using only an acidic aqueous solution containing citric acid monohydrate and nickel nitrate hexahydrate (N$_2$NiO$_6$ x H$_2$O) to impregnate the δ-Al$_2$O$_3$, which resulted in 8.4 wt% nominal loading of elemental Ni on the support. The same procedure of aging, drying, and calcination was used as for other catalysts. Finally, catalyst S6 was prepared by impregnation of an aqueous solution of ammonium heptamolybdate tetrahydrate (H$_{24}$Mo$_7$N$_6$O$_{24}$×4H$_2$O) onto δ-Al$_2$O$_3$ support with the same aging, drying, and calcination procedure as above, resulting in 14 wt% nominal loading of elemental Mo. The samples were characterized using energy-dispersive X-ray spectroscopy (EDX) in scanning transmission electron microscopy (STEM) mode. Images can be found in a previous publication [24]. The composition of the NiMo catalyst supported on SiO$_2$ was analyzed using EDX in a scanning electron microscopy (SEM) instrument. Loadings estimated from EDX for all catalysts are reported in Table 1.

2.2 In Situ Experiments

XAFS measurements were performed at the ROCK beamline at Synchrotron SOLEIL in France. Ni K-edge (8332.8 eV) and Mo K-edge (19,999.5 eV) spectra were measured alternately using the ROCK Quick-XAS [34–37] set up with two independent monochromators and sets of ion chambers, allowing rapid jumps between edges. With this setup, we were able to measure both edges repeatedly with a total cycle time of the 90 s [34]. The absorption Ni K-edge spectra were measured using Si(111) and Mo K-edge spectra were measured using Si(220) monochromator crystals. Mirrors at a 2.8 mrad grazing incidence were used with B4C and Pd stripes for harmonic rejection at the Ni K-edge and Mo K-edge, respectively.

The catalysts were ground to a powder and loaded into a quartz capillary (1.5 mm in outer diameter with a wall thickness of 0.01 mm). The spectra were recorded in transmission mode and the temperature was increased at the rate of 3 °C/min from room temperature (RT) to 400 °C in 10% H$_2$S/H$_2$ (7 mL/min) at 2 and 10 bar total pressure. When 400 °C was reached, the sample was kept in sulfidizing conditions for 2 h before it was cooled down to RT at the rate of 5 °C/min. Heating was provided by a hot air gun placed underneath the capillary reactor, a thermocouple used for temperature measurement was placed in the middle of the glass capillary, in contact with the catalyst. A mass spectrometer (MKS Cirrus) was installed at the outlet of the gas line to verify flow of the correct gases through the cell and to record the times at which gas changes occurred. MoO$_2$, MoO$_3$, MoS$_2$, NiO and Ni$_3$S$_2$ reference materials (> 99%) were pressed into pellets with boron nitride as binder and measured in transmission at room temperature.

The Larch [38] package was used for XAFS data processing and analysis, and EXAFS fits were performed using the implementation of IFEFFIT [39] included in this package.

Spectra were fitted using single-scattering paths calculated for MoO$_3$, MoS$_2$, NiO and Ni$_3$S$_2$ using FEFF9.6. [40] The k-range was 3–13 Å^{-1} for all fits and R-ranges were set to 1–2.0 Å and 1–2.1 Å for Mo and Ni oxidized states, respectively and 1–3.4 Å for the sulfidized states (Fig. 1).

3 Results and Discussion

3.1 Molybdenum K-Edge XAFS

Figure 2a shows the initial state of Mo-containing catalysts and references for oxidized Mo compounds, measured in He before sulfidation. XANES spectra for all catalysts display a shape characteristic of hexavalent Mo oxidic species characteristic of non centrosymmetric geometry, as verified for instance for MoO$_3$ (shown) or polymolybdate (not shown) species [41, 42]. EXAFS spectra show a dominant oxygen component at ~ 1.2 Å (without phase correction) in the Fourier transform (FT). Fit results (Figure S2a, b and Table S1 in Supplementary information) show similar
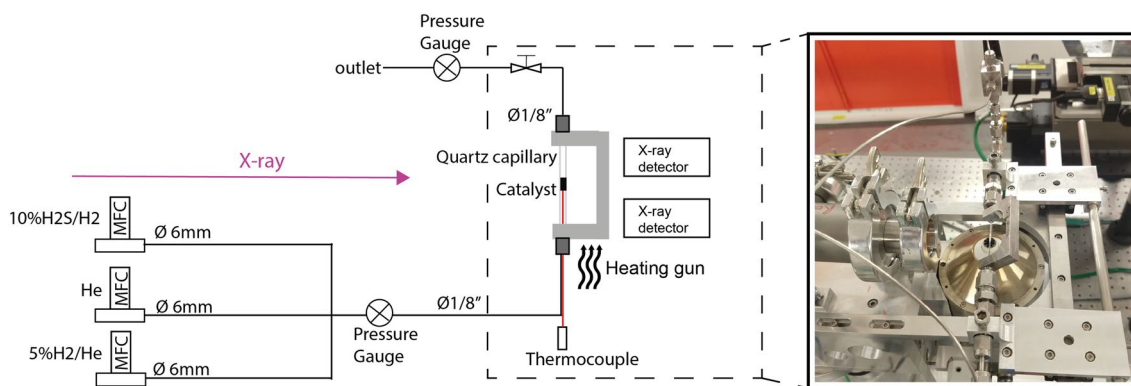
Fig. 1 A schematic of the XAFS setup at the beamline ROCK at Soleil. To the right is a photo of the quartz capillary used as a reactor with a heating gun positioned underneath
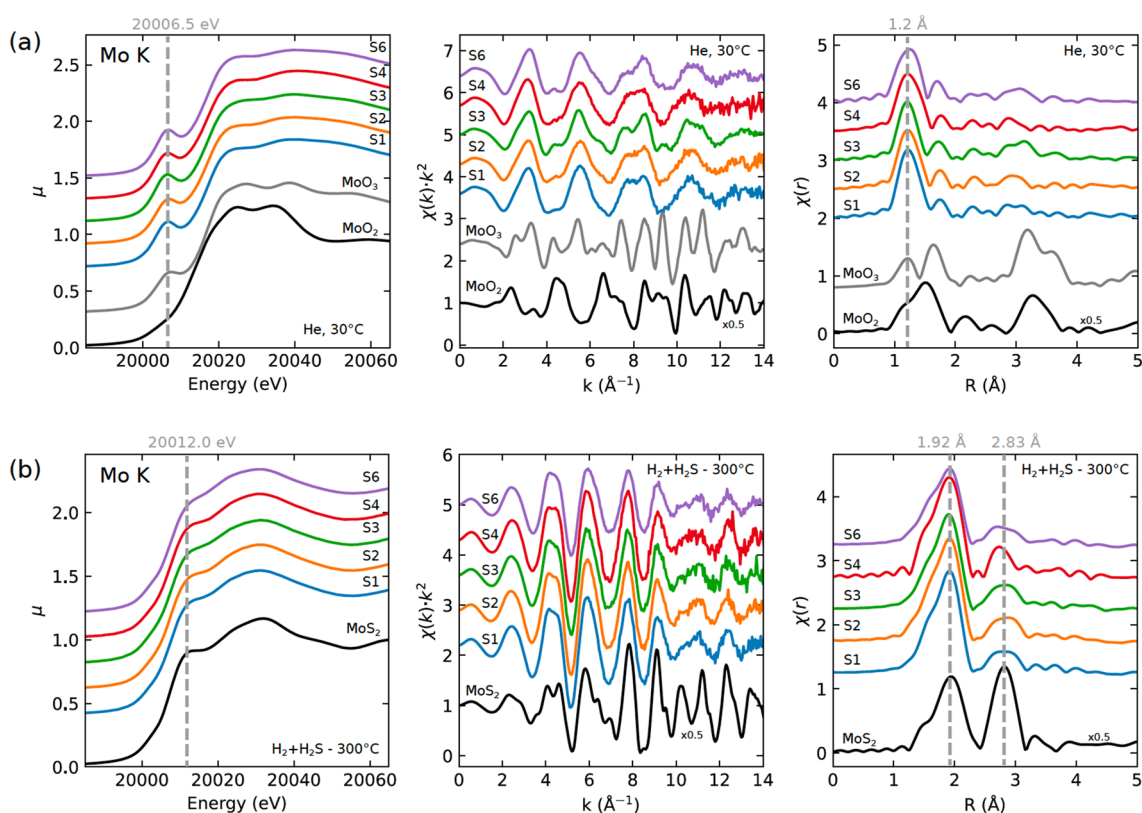

Fig. 2 XANES (left) and EXAFS (middle, right, k^2-weighting) spectra for the various catalysts acquired before the experiments (in He at ~ 30 °C) and after sulfidation (in H_2S/H_2 at ~ 300 °C). **a** Mo K-edge spectra before sulfidation. **b** Mo K-edge spectra after sulfidation. Gray dashed lines show the positions of characteristic features of MoO_3 and MoS_2 reference spectra

Mo–O distances, 1.71–1.73 Å, for all catalysts consistent with previous reports [43]. Figure 2b shows the Mo K-edge spectra measured at 300 °C, which is considered to be the final state of the Mo-containing catalysts. Between 300 and 400 °C no significant changes could be observed in the spectra. XANES spectra are similar to MoS_2 spectra and FT of EXAFS spectra display for all catalysts a Mo–S first

coordination shell contribution and a Mo–Mo component. No significant difference has been observed for Mo species on Al_2O_3 and SiO_2 supports as well as for measurements performed at different pressures. Spectra from the samples after sulfidation could be fitted well with Mo–S and Mo–Mo scattering paths and results are shown in the Supplementary information in Figure S1c, d and Table S2. Consistent
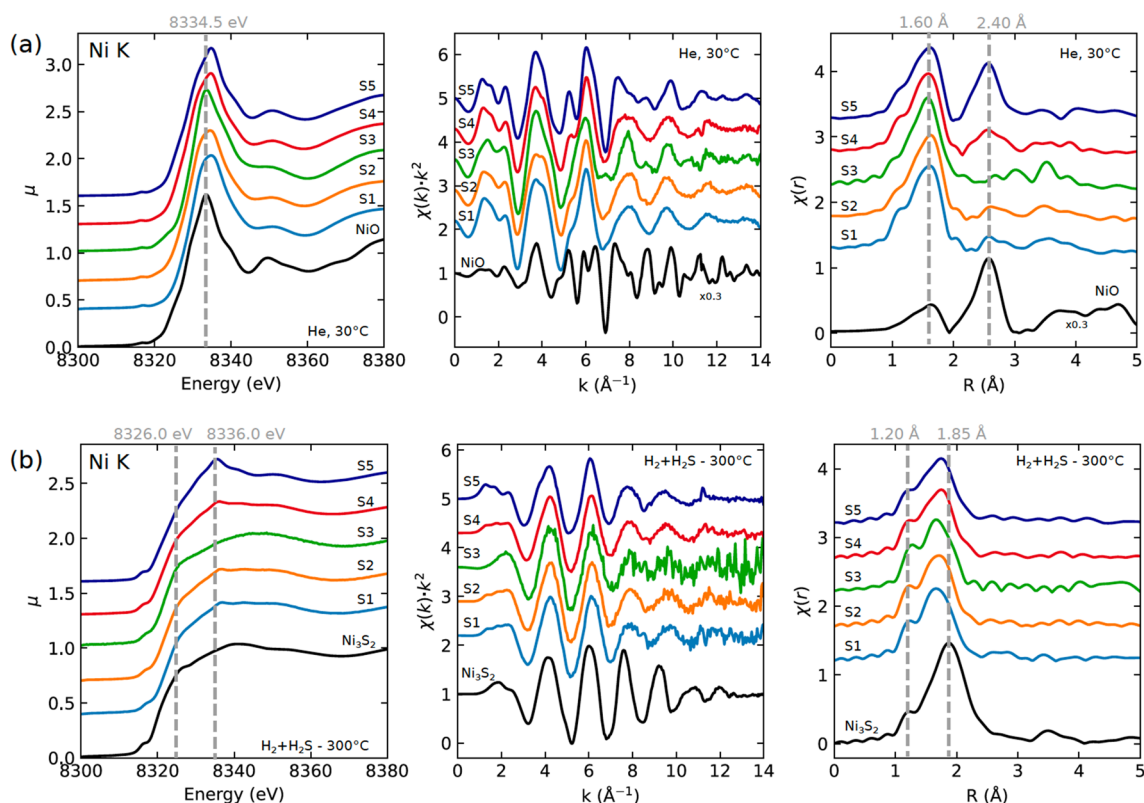
Fig. 3 XANES (left) and EXAFS (middle, right, k2-weighting) spectra for the various catalysts acquired before the experiments (in He at ~ 30 °C) and after sulfidation (in H_2S/H_2 at ~ 300 °C). **a** Ni K-edge spectra before sulfidation. **b** Ni K-edge spectra after sulfidation. Gray dashed lines show the positions of characteristic features of NiO and Ni_3S_2 reference spectra

Mo–S and Mo–Mo distances were found for all catalysts, about 2.42 Å and 3.19 Å, respectively which agrees with previously reported distances for MoS_2 [44, 45]. The fitted coordination numbers and scattering distances for all catalysts after sulfidation are in agreement with what has previously been reported for molybdenum sulfide catalysts on γ-Al_2O_3. [45]

3.2 Nickel K-Edge XAFS

The initial state of Ni-containing catalysts is shown in Fig. 3a with positions of characteristic features for reference spectra NiO and Ni_3S_2 indicated with a gray dashed line. Some variations can be observed in the XANES spectra from different samples at the beginning of the sulfidation process, however, all spectra resemble that of NiO. The most pronounced difference is observed by comparing samples S1 and S3, consisting of catalysts with different supports. The SiO_2-supported catalyst (S3) shows a shoulder in the rising edge at 8321 eV (Fig. 3a) which is not common for NiO or observed in other samples. Catalysts with the highest Ni loading (S4 and S5) show a XANES peak at the highest energy position and have a more pronounced Ni–Ni component in EXAFS compared to other

catalysts which is observed in EXAFS spectra (Fig. 3a—right) at around 2.4 Å. Figure 3b shows the final state of Ni-containing catalysts. At higher temperatures no noticeable changes could be observed in the spectra. Significant differences can be observed in XANES for all catalysts of which the most pronounced is again caused by the effect of the support. Catalyst S3, supported on SiO_2, shows the greatest similarity to reference Ni_3S_2 spectra with a characteristic shoulder (~ 8326 eV, marked in Fig. 3b) and absence of the peak at around 8336 eV (marked in Fig. 3b). Again, catalysts with the highest Ni loading (S4 and S5) show the most prominent peak (~ 8336 eV, marked in Fig. 3b) which might be attributed to the presence of the oxidized state of the sample and implying a lesser degree of sulfidation than for other catalysts. EXAFS spectra show Ni-S components present in all catalysts post sulfidation. Ni K-edge EXAFS fits are shown in Supplementary Information in Figure S3c, d. The fit results for Ni-containing catalysts before and after sulfidation are shown in Supplementary Information in Table S3 and Table S4, respectively. The most pronounced peak for measurements at the beginning of the sulfidation corresponds to the Ni–O path with the distance of 2.02 Å, found by the EXAFS fits for samples S1–S3, and agrees well with previously reported data [43]. However, inclusion of

Fig. 4 XAFS spectra recorded for catalyst S1 during sulfidation. Mo and Ni spectra were measured alternately on the same catalyst during the same ramp. For clarity, only every 5th spectrum is plotted. **a** Mo K-edge XANES, **b** Mo K-edge EXAFS, **c** Ni K-edge XANES, **d** Ni K-edge EXAFS. Features used for tracking the temperature-dependent behavior are indicated (gray)
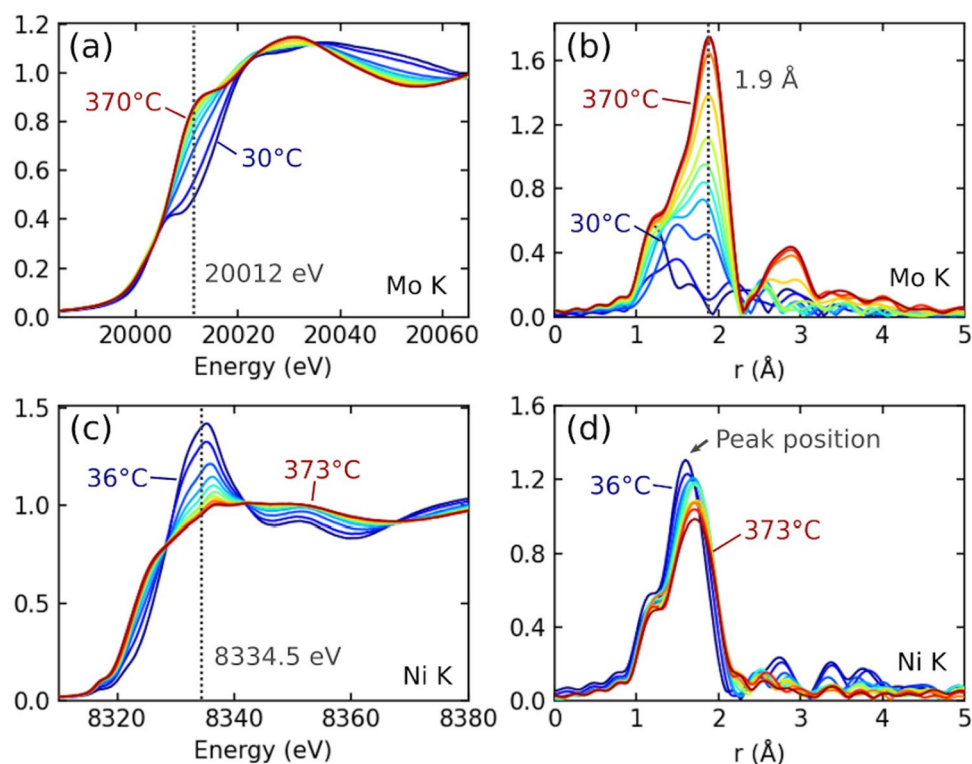
Ni–Ni scattering path from NiO was necessary for samples S4 and S5 which indicates presence of significant amounts of bulk NiO in these samples. Ni–S scattering path was sufficient to fit post-sulfidized spectra giving an average Ni–S distance of 2.21 Å, which agrees with previously reported Ni–S distances for sulfidized NiMo catalysts [37, 43].

3.3 In Situ Sulfidation

Changes observed in XANES and EXAFS spectra during temperature increases are consistent with transitions from oxidized to sulfidized structures for both Mo and Ni species. Figure 4 shows spectra acquired for catalyst S1, as an example of in situ sulfidation. Previous studies [37, 46–49] have shown that sulfidation follows a multiple-step process with several intermediates. For simplicity and to allow comparison between the different catalysts, we track characteristic features of the XANES and EXAFS spectra (Figs. 4, 5). For Mo, we follow the growth of the shoulder at 20012.0 eV in XANES (Fig. 4a) as well as the magnitude of the Fourier-transform signal at 1.9 Å (Fig. 4b), both of which are associated with the formation of the sulfide. For Ni, we track the XANES intensity at the position of the NiO white line at 8334.5 eV (Fig. 4c). As the Ni–O and Ni–S components overlap strongly in the EXAFS Fourier-transform spectra, the intensity was not a useful quantity; instead, we track the position of the peak maximum (Fig. 4d).

The comparison of spectra from different samples during sulfidation is shown in Fig. 5. The sulfidation of Mo is similar for all samples except for sample S6 (Mo/Al_2O_3) which is sulfidized less readily. Similarly, Fig. 5b shows the magnitude of the Mo K-edge EXAFS component corresponding to the Mo-S scattering at 1.9 Å. It is observed that the sulfidation reaction for all samples happens in two steps and when correlated with the intensities from XANES, most of the conversion to a sulfide occurs below 150 °C. EXAFS fits for samples S1–S4 at 200 °C (Table S5 in the Supplementary Information) gave a coordination number (N) of Mo-S close to 6, I.e. the same as in bulk MoS_2, and remains constant with temperature while the Debye–Waller factor decreases. This indicates that the second step in sulfidation is not a reaction with sulfur but ordering of the sulfide species or clusters. The absence of Ni in sample S6, together with the lesser sulfidation degree of this sample, found from XANES, corresponds well with the hypothesis that the addition of Ni promoters lowers the sulfidation temperature [20, 45]. No significant differences are observed in the Mo sulfidation for different supports (samples S1 vs. S3) or different Ni:Mo ratios (S1 vs S4), or between sulfidation processes carried out at different total pressures (S1 vs. S2).

The trends obtained from Ni spectra (Fig. 5c, d) show much more variability among the catalysts compared to Mo spectra. The trends for Ni, based on the intensity at 8334.5 eV (Fig. 5c), show very similar behavior for samples S1, S2 and S4, the main differences being likely related to the initial white line intensity. Sample S4, with a higher

Fig. 5 Comparison of spectra from different samples during sulfidation. **a** Plot of the Mo K-edge XANES intensity at 20012.0 eV. **b** Magnitude of the Mo-K-edge EXAFS component corresponding to Mo-S scattering. **c** Plot of the Ni K-edge XANES intensity at 8334.5 eV, corresponding approximately to the white line maximum for oxidized samples. **d** Position of the peak maximum in the Ni K-edge EXAFS spectrum, which corresponds to overlapping Ni–O and Ni–S scattering components
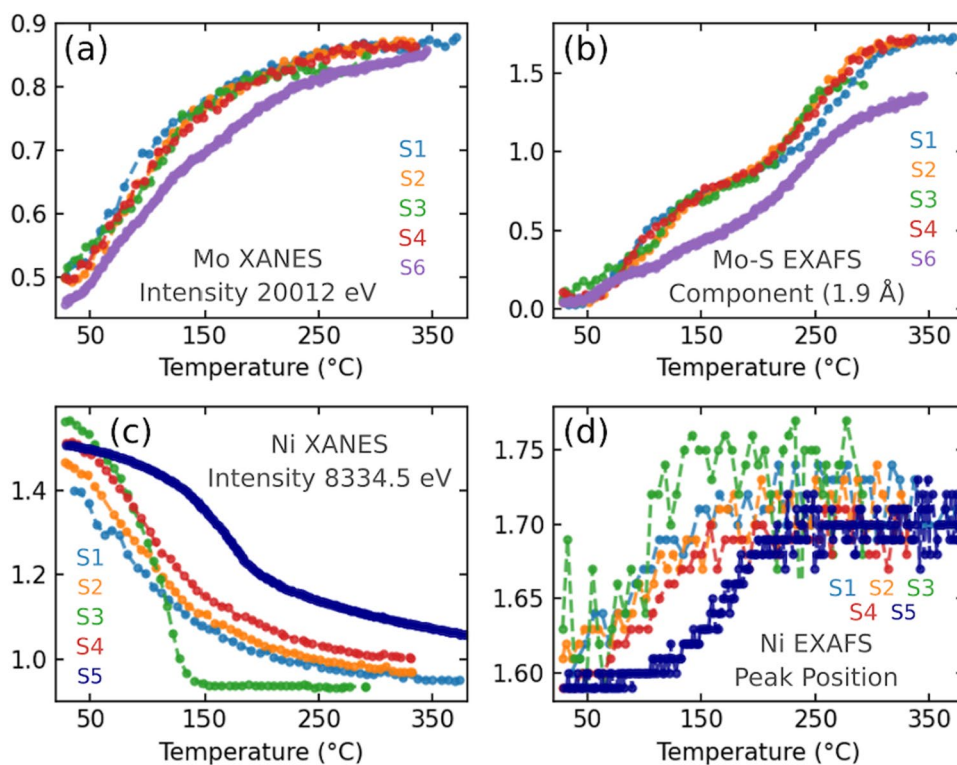
loading of Ni, is converted to sulfide at a slightly higher temperature as can be seen more clearly by the position of peak maximum in EXAFS spectrum corresponding to overlapping Ni–O and Ni–S scattering components (Fig. 5d). This difference can be attributed to the location of Ni atoms in the sample, as suggested by Liu et al. [50]. They found that lower Ni loading and calcination at 500 °C result in surface Ni atoms with high activity toward sulfidation due to their availability. However, higher loading of Ni resulted in the embedding of the Ni atoms into the alumina support possibly causing a lower tendency for sulfidation reaction [50]. Similar to the monometallic Mo sample (S6), the monometallic Ni sample (S5) shows to be much less readily sulfidized compared to any of the bimetallic catalysts; the sulfidation takes place nearly 100 °C higher in temperature than what is observed for S1, for example. This further confirms the importance of the two metals in facilitating catalyst activation.

In contrast to what is observed for Mo, a big difference in sulfidation behavior of Ni is observed depending on the support used (S1 vs S3). Sample S3 with SiO_2 support is much more readily sulfidized than sample S1 with δ-Al_2O_3 support but with the same Ni:Mo ratio. This can be observed from both XANES and EXAFS trends where a complete conversion occurs before 150 °C for sample S3 while sulfidation of all the Al_2O_3-supported catalysts shows an incomplete sulfidation even at the highest temperatures. This behavior is indicative of a strong interaction between the oxidized Ni and the Al_2O_3 support, and possibly even the formation of

the $NiAl_2O_4$ spinel compound [50–54]. Similar compound formation does not occur with SiO_2. The shift to lower onset temperature of the sulfidation with increasing amounts of Mo for Al_2O_3 supported catalysts may also be caused in part by the latter metal hindering this reaction, although larger NiO particle size with higher loading (evident in the 2.5 Å EXAFS component, Fig. 3a) may also play a role. In any case, the more facile sulfidization observed for the SiO_2-supported catalyst suggests this may be advantageous for HDO reactions. However, it has been reported that such catalysts show lower activity related to the weaker interactions with the support, which fails to prevent sintering [55]. The stronger interaction with the Al_2O_3 support prevents the sintering and thus stabilizes the catalyst [18, 20–22].

4 Conclusions

In this work, a series of Ni, Mo and NiMo catalysts were prepared by incipient wetness impregnation and characterized by Quick-XAS during sulfidation reaction in H_2S/H_2. The XAFS analysis suggests that all samples have Mo and Ni species present in oxide phases at the beginning of the sulfidation reaction. It is found that monometallic samples are less readily sulfidized than the bimetallic ones, suggesting the importance of Ni-Mo interaction in the activity of the catalyst, meaning the active phase is formed at lower temperatures which are of high importance for industrial

processes. Detailed analysis of Mo K-edge XAFS data revealed that sulfidation evolves in two steps, where most of the oxide is converted into sulfide below 150 °C. No significant difference was observed in the Mo K-edge spectra measured at NiMo catalysts with different supports. Ni K-edge spectra show similar behavior for samples supported on δ-Al$_2$O$_3$ with a small difference based on the Ni loading—higher loading resulted in a slightly lower degree of sulfidation than lower loading, suggesting possible embedding of Ni to the support due to strong interactions. Furthermore, higher Ni loading may result in the formation of larger Ni particles that are harder to sulfidize. The catalyst supported on SiO$_2$ seemingly showed a higher tendency for the sulfidation reaction based on Ni K-edge spectra which may be advantageous for HDO reactions. Nevertheless, the strong interaction with Al$_2$O$_3$ support is more promising since it prevents sintering and thus stabilizes the catalyst.

The results demonstrate the effect of different parameters on sulfidation, especially the importance of NiMo interactions for these industrial processes due to the different behavior during sulfidation compared to monometallic catalysts. Therefore, these results are contributing to the understanding of the formation of the active sites which should be considered when producing future Mo-based catalysts.

References

1. European Environment Agency (2022) https://www.eea.europa.eu/ims/greenhouse-gas-emissions-from-transport. Acessed 20 July 2022

2. Zeng L, Cheng CY (2009) A literature review of the recovery of molybdenum and vanadium from spent hydrodesulphurisation catalysts: Part I: Metallurgical processes. Hydrometallurgy 98:1–9

3. Souza PM, Rabelo-Neto RC, Borges LEP, Jacobs G, Davis BH, Sooknoi T, Resasco DE, Noronha FB (2015) Role of keto intermediates in the hydrodeoxygenation of phenol over Pd on oxophilic supports. ACS Catal 5:1318–1329

4. Topsøe H, Clausen BS, Candia R, Wivel C, Mørup S (1981) In situ Mössbauer emission spectroscopy studies of unsupported and supported sulfided Co-Mo hydrodesulfurization catalysts: evidence for and nature of a Co-Mo-S phase. J Catal 68:433–452

5. Mortensen PM, Grunwaldt JD, Jensen PA, Knudsen KG, Jensen AD (2011) A review of catalytic upgrading of bio-oil to engine fuels. Appl Catal A 407:1–19

6. Sotelo-Boyás R, Liu Y, Minowa T (2011) Renewable diesel production from the hydrotreating of rapeseed oil with Pt/Zeolite and NiMo/Al$_2$O$_3$ catalysts. Ind Eng Chem Res 50:2791–2799

7. Ameen M, Azizan MT, Ramli A, Yusup S, Abdullah B (2020) The effect of metal loading over Ni/γ-Al$_2$O$_3$ and Mo/γ-Al$_2$O$_3$ catalysts on reaction routes of hydrodeoxygenation of rubber seed oil for green diesel production. Catal 355:51–64

8. Mom RV, Louwen JN, Frenken JWM, Groot IMN (2019) In situ observations of an active MoS$_2$ model hydrodesulfurization catalyst. Nat Commun 10:2546–2552

9. Helveg S, Lauritsen JV, Laegsgaard E, Stensgaard II, Norskov JK, Clausen BS, Topsoe H, Besenbacher F (2000) Atomic-scale structure of single-layer MoS$_2$ nanoclusters. Phys Rev Lett 84:951–954

10. Bruix A, Füchtbauer HG, Tuxen AK, Walton AS, Andersen M, Porsgaard S, Besenbacher F, Hammer B, Lauritsen JV (2015) In situ detection of active edge sites in single-layer MoS$_2$ catalysts. ACS Nano 9:9322–9330

11. Hansen LP, Ramasse QM, Kisielowski C, Brorson M, Johnson E, Topsøe H, Helveg S (2011) Atomic-scale edge structures on industrial-style MoS$_2$ nanocatalysts. Angew Chem Int Ed 50:10153–10156

12. Salazar N, Beinik I, Lauritsen JV (2017) Single-layer MoS$_2$ formation by sulfidation of molybdenum oxides in different oxidation states on Au(111). Phys Chem Chem Phys 19:14020–14029

13. Lauritsen JV, Kibsgaard J, Helveg S, Topsøe H, Clausen BS, Lægsgaard E, Besenbacher F (2007) Size-dependent structure of MoS$_2$ nanocrystals. Nat Nanotechnol 2:53–58

14. Hu J, Yu L, Deng J, Wang Y, Cheng K, Ma C, Zhang Q, Wen W, Yu S, Pan Y, Yang J, Ma H, Qi F, Wang Y, Zheng Y, Chen M, Huang R, Zhang S, Zhao Z, Deng D (2021) Sulfur vacancy-rich MoS$_2$ as a catalyst for the hydrogenation of CO$_2$ to methanol. Nat Catal 4:242–250

15. Brito J, Laine J (1986) Characterization of supported MoO$_3$ by temperature-programmed reduction. Polyhedron 5:179–182

16. Gangwar J, Gupta BK, Tripathi SK, Srivastava AK (2015) Phase dependent thermal and spectroscopic responses of Al$_2$O$_3$ nanostructures with different morphogenesis. Nanoscale 7:13313–13344

17. Kovarik L, Bowden M, Genc A, Szanyi J, Peden CFH, Kwak JH (2014) Structure of δ-alumina: toward the atomic level understanding of transition alumina phases. J Phys Chem C 118:18051–18058

18. Wang X, Zhao Z, Zheng P, Chen Z, Duan A, Xu C, Jiao J, Zhang H, Cao Z, Ge B (2016) Synthesis of NiMo catalysts supported on mesoporous Al$_2$O$_3$ with different crystal forms and superior catalytic performance for the hydrodesulfurization of dibenzothiophene and 4,6-dimethyldibenzothiophene. J Catal 344:680–691

19. Furimsky E (2000) Catalytic hydrodeoxygenation. Appl Catal A 199:147–190

20. Topsøe H, Clausen BS, Topsøe NY, Zeuthen P (1989) Progress in the design of hydrotreating catalysts based on fundamental molecular insight. Stud Surf Sci Catal 53:77–102

21. Aksoylu AE, Önsan ZI (1998) Interaction between Nickel and Molybdenum in Ni–Mo/Al$_2$O$_3$ catalysts: II: CO hydrogenation. Appl Catal A 168:399–407

22. Koklyukhin AS, Mozhaev AV, Sal'nikov VA, Nikul'shin PA (2017) Promoter nature effect on the sensitivity of Ni-Mo/Al$_2$O$_3$, Co-Mo/Al$_2$O$_3$, and Ni-Co-Mo/Al$_2$O$_3$ catalysts to dodecanoic acid in the co-hydrotreating of dibenzothiophene and naphthalene. Kinet Catal 58:463–470

23. Muhammad Y, Rashid HU, Subhan S, Rahman AU, Sahibzada M, Tong Z (2019) Boosting the hydrodesulfurization of dibenzothiophene efficiency of Mn decorated (Co/Ni)-Mo/Al$_2$O$_3$ catalysts at mild temperature and pressure by coupling with phosphonium based ionic liquids. Chem Eng J 375:121957

24. Gericke SM, Rissler J, Bermeo M, Wallander H, Karlsson H, Kollberg L, Scardamaglia M, Temperton R, Zhu S, Sigfridsson Clauss KV, Hulteberg C, Shavorskiy A, Merte LR, Messing ME, Zetterberg J, Blomberg S (2022) In situ H$_2$ reduction of Al$_2$O$_3$-supported Ni- and Mo-based catalysts. Catalysts 12:755–770

25. Qu L, Zhang W, Kooyman PJ, Prins R (2003) MAS NMR, TPR, and TEM studies of the interaction of NiMo with alumina and silica–alumina supports. J Catal 215:7–13

26. Qian W, Hachiya Y, Wang D, Hirabayashi K, Ishihara A, Kabe T, Okazaki H, Adachi M (2002) Elucidation of promotion effect of nickel on Mo/Al$_2$O$_3$ and Co-Mo/Al$_2$O$_3$ catalysts in hydrodesulfurization using a 35S radioisotope tracer method. Appl Catal A 227:19–28

27. Hong ST, Park DR, Yoo SJ, Kim JD, Park HS (2006) Characterization of the active phase of NiMo/Al$_2$O$_3$ hydrodesulfurization catalysts. Res Chem Intermed 32:857–870

28. Topsøe H (2003) Developments in operando studies and in situ characterization of heterogeneous catalysts. J Catal 216:155–164

29. Timoshenko J, Roldan Cuenya B (2021) In situ/operando electrocatalyst characterization by X-ray absorption spectroscopy. Chem Rev 121:882–961

30. Newville M (2004) Fundamentals of XAFS. Consortium for Advanced Radiation Sources, University of Chicago (USA)

31. Lytle FW (1999) The EXAFS family tree: a personal history of the development of extended X-ray absorption fine structure. J Synchrotron Radiat 6:123–134

32. Koningsberger DC, Mojet B, Van Dorssen G, Ramaker DE (2000) XAFS spectroscopy: fundamental principles and data analysis. Top Catal 10:143–155

33. Blomberg S, Johansson N, Kokkonen E, Rissler J, Kollberg L, Preger C, Franzén SM, Messing ME, Hulteberg C (2019) Bimetallic nanoparticles as a model system for an industrial NiMo catalyst. Materials 12:3727–3740

34. Briois V, Fontaine CL, Belin S, Barthe L, Moreno T, Pinty V, Carcy A, Girardot R, Fonda E (2016) ROCK: the new Quick-EXAFS beamline at SOLEIL. J Phys Conf Ser 712:012149

35. Briois V, Fonda E, Belin S, Barthe L, Fontaine CL, Langlois F, Ribbens M, Villain F (2011) SAMBA: The 4–40 keV X-ray absorption spectroscopy beamline at SOLEIL. App Dev Sci 41–47

36. Fonda E, Rochet A, Ribbens M, Barthe L, Belin S, Briois V (2012) The SAMBA quick-EXAFS monochromator: XAS with edge jumping. J Synchrotron Rad 19:417–424

37. Rochet A, Baubet B, Moizan V, Devers E, Hugon A, Pichon C, Payen E, Briois V (2017) Intermediate species revealed during sulfidation of bimetallic hydrotreating catalyst: a multivariate analysis of combined time-resolved spectroscopies. J Phys Chem C 121:18544–18556

38. Newville M (2013) Larch: an analysis package for XAFS and related spectroscopies. J Phys Conf Ser 430:012007

39. Newville M (2001) IFEFFIT: interactive XAFS analysis and FEFF fitting. J Synchrotron Rad 8:322–324

40. Rehr JJ, Kas JJ, Vila FD, Prange MP, Jorissen K (2010) Parameter-free calculations of X-ray spectra with FEFF9. Phys Chem Chem Phys 12:5503–5513

41. Ressler T, Timpe O, Neisius T, Find J, Mestl G, Dieterle M, Schlögl R (2000) Time-resolved XAS investigation of the reduction/oxidation of MoO$_{3-x}$. J Catal 191:75–85

42. Reschke S, Niks D, Wilson H, Sigfridsson KGV, Haumann M, Rajagopalan KV, Hille R, Leimkühler S (2013) Effect of exchange of the cysteine molybdenum ligand with selenocysteine on the structure and function of the active site in human sulfite oxidase. Biochemistry 52:8295–8303

43. Rochet A, Baubet B, Moizan V, Devers E, Hugon A, Pichon C, Payen E, Briois V (2015) Influence of the preparation conditions of oxidic NiMo/Al$_2$O$_3$ catalysts on the sulfidation ability: a quick-XAS and Raman Spectroscopic Study. J Phys Chem C 119:23928–23942

44. Joensen P, Crozier ED, Alberding N, Frindt RF (1987) A study of single-layer and restacked MoS$_2$ by X-ray diffraction and X-ray absorption spectroscopy. J Phys C 20:4043–4053

45. Shimada H, Matsubayashi N, Sato T et al (1993) EXAFS study on the dispersion of molybdenum sulfide catalysts on γ-Al$_2$O$_3$. Catal Lett 20:81–86

46. Dupont C, Lemeur R, Daudin A, Raybaud P (2011) Hydrodeoxygenation pathways catalyzed by MoS$_2$ and NiMoS active phases: A DFT study. J Catal 279:276–286

47. Jong AM, Borg HJ, IJzendoorn LJ, Soudant VGFM, Beer VHJ, Veen JAR, Niemantsverdriet JW (1993) Sulfidation mechanism by molybdenum catalysts supported on silica/silicon(100) model support studied by surface spectroscopy. J Phys Chem 97:6477–6483

48. Lesage C, Devers E, Legens C, Fernandes G, Roudenko O, Briois V (2019) High pressure cell for edge Jumping X-ray absorption spectroscopy: applications to industrial liquid sulfidation of hydrotreatment catalysts. Catal Today 336:63–73

49. Rochet A, Baubet B, Moizan V, Pichon C, Briois V (2016) Co-K and Mo K edges Quick-XAS study of the sulphidation properties of Mo/Al$_2$O$_3$ and CoMo/Al$_2$O$_3$ catalysts. C R Chim 19(10):1337–1351

50. Liu Z, Han W, Hu D, Sun S, Hu A, Wang Z, Jia Y, Zhao X, Yang Q (2020) Effects of Ni–Al$_2$O$_3$ interaction on NiMo/Al$_2$O$_3$ hydrodesulfurization catalysts. J Catal 387:62–72

51. Dufresne P, Payen E, Grimblot J, Bonnelle JP (1981) Study of Ni-Mo-γ-Al$_2$O$_3$ catalysts by x-ray photoelectron and Raman spectroscopy. Comparison with Co-Mo- γ-Al$_2$O$_3$ catalysts. J Phys Chem 85:2344–2351

52. Salagre P, Fierro JLG, Medina F, Sueiras JE (1996) Characterization of nickel species on several γ-alumina supported nickel samples. J Mol Catal A 106:125–134

53. Hernández-Huesca R, Mérida-Robles J, Maireles-Torres P, Rodríguez-Castellón E, Jiménez-López A (2001) hydrogenation and ring-opening of tetralin on Ni and NiMo supported on alumina-pillared α-zirconium phosphate catalysts. A thiotolerance study. J Catal 203:122–132

54. Liu F, Xu S, Cao L, Chi Y, Zhang T, Xue D (2007) A comparison of NiMo/Al$_2$O$_3$ catalysts prepared by impregnation and coprecipitation methods for hydrodesulfurization of dibenzothiophene. J Phys Chem C 111:7396–7402

55. Cattaneo R, Shido T, Prins R (1999) The relationship between the structure of NiMo/SiO$_2$ catalyst precursors prepared in the presence of chelating ligands and the hydrodesulfurization activity of the final sulfided catalysts. J Catal 185:199–212